Direct Evidence for Active Support Participation in Oxide Catalysis: Multiple *Operando* Spectroscopy of VO_x/Ceria

Patrick Ober[†], Simone Rogg[†], Christian Hess*

Eduard-Zintl-Institut für Anorganische und Physikalische Chemie, Technische Universität Darmstadt, Alarich-Weiss-Str. 8, 64287 Darmstadt, Germany

*Corresponding Author (E-mail: hess@pc.chemie.tu-darmstadt.de)

† These two authors contributed equally

Abstract

Ceria-supported vanadia is catalytically active in oxidative dehydrogenation (ODH) reactions. Here, we provide direct spectroscopic evidence for the participation of the ceria support in the redox catalysis. To unravel the structural dynamics of vanadia/ceria (VO_x/CeO_2) catalysts during ethanol ODH, we have applied a combination of *operando* multi-wavelength Raman and *operando* UV-Vis spectroscopy. Our approach consists in the targeted use of different Raman excitation wavelengths, enabling the selective enhancement of ceria (at 385 nm) and vanadia (at 515 nm) vibrational features. As part of the support dynamics, ceria lattice oxygen is shown to directly participate in the ODH reaction, while V-O-Ce interface bonds are broken during substrate adsorption, resulting in ethoxide formation. The presence of V-O-Ce bonds is considered to be crucial for the observed synergy effect in catalytic performance, allowing ceria to act as an oxygen buffer stabilizing the vanadium center. By providing an experimental basis for a detailed understanding of working VO_x/CeO_2 catalysts, our results highlight the importance of active support participation in oxide catalysis.

Keywords: active support, oxide catalysis, oxidative dehydrogenation, operando spectroscopy, vanadia, ceria

1. Introduction

Supported vanadia is the catalyst for the oxidative dehydrogenation (ODH) of alcohols and short-chain alkanes that has been studied most with the overall objective of establishing a different approach for the production of propylene or ethylene as an alternative to conventional processes such as steam cracking.[1–4] The support material has been shown to have an enormous impact on the activity and selectivity of vanadia catalysts, and may be classified as being inactive (SiO_2, Al_2O_3) or active (TiO_2, CeO_2).[1,2,5,6] Active support materials are characterized by their reducibility and have been proposed to directly participate in the redox cycle.[1,6–10] However, primary experimental evidence for their participation, e.g. by in situ/*operando* spectroscopy, is scarce.[11–14]

Recently, ceria-supported vanadia (VO_x/CeO_2) has attracted considerable attention as a promising alternative catalyst for ODH reactions.[7,11,12,15–20] In the context of alcohol ODH, experimental and, in particular, theoretical studies have been carried out to gain a deeper understanding of the support interaction in VO_x/CeO_2 systems.[10,21–24] According to combined experimental and density functional theory (DFT) studies on $VO_x/CeO_2(111)$,[10,21] ceria stabilizes small vanadia species in a +5 oxidation state, which are proposed to wet and reduce the ceria surface. Using DFT, Kropp and Paier[22] postulated a mechanism for methanol ODH over $CeO_2(111)$-supported vanadia monomers, starting with methanol chemisorption either at the V-O-Ce interface bond or at a pseudo-vacancy of the ceria surface. According to the first scenario, after a V-O-CH_3 structure has been formed, dehydrogenation occurs via interaction of methoxy with a ceria surface oxygen, whereas, in the second scenario, methoxy adsorbed on ceria transfers an H atom to the V-O-Ce interface bond. In a subsequent study, the adsorption and partial oxidation of methanol at a trimeric VO_x species on $CeO_2(111)$ was studied, which, however, was found to exhibit a lower activity than the monomer due to structural relaxation in the surface O layer of the latter.[23] In another DFT study, Wu and Gong[24] explicitly examined various oxygen species of $VO_x/CeO_2(111)$ containing vanadia monomers and derived a

structural evolution of VO_x species during methanol ODH. The V-O-Ce unit of metastable VO_4 species was proven to be the most favorable site for the rate-limiting C-H bond breakage. New empty localized states generated by the vanadia deposition served as an explanation for the synergic effect of the vanadia/ceria system. To the best of our knowledge, there has been no experimental evaluation of these theoretical proposals.

In this study, we have addressed the role of the support in VO_x/CeO_2 catalysts by applying a combination of *operando* multi-wavelength Raman and *operando* UV-Vis spectroscopy during ethanol ODH. This approach enables us to unravel the structural dynamics of VO_x/CeO_2 catalysts under working conditions and to provide direct spectroscopic evidence for the participation of the ceria support in the redox catalysis. The targeted use of multi-wavelength Raman spectroscopy is essential for the selective enhancement of ceria and vanadia vibrational features. While its potential has been demonstrated previously for structural characterization of supported vanadia catalysts both under non-reactive[25] and under reactive conditions,[26] there have been no in situ or *operando* studies on active support participation in oxide catalysis.

2. Experimental

Catalyst preparation. Ceria was synthesized as described previously[27] and loaded with vanadium oxide by incipient wetness impregnation. The impregnation was performed by mixing 2 g of ceria with 0.5 mL of the precursor solution of vanadium(V) oxytriisopropoxide (≥97%, Sigma Aldrich) and 2-propanol (99.5%, Sigma Aldrich) (concentration: 0.5 mol/l). Subsequently, the sample was heated to 500 °C at a heating rate of 1.5 °C min^{-1} and calcined at 500 °C for 12 h. The specific surface area of ceria was determined to be 62.3 $m^2 g^{-1}$, as determined by the Brunauer–Emmett–Teller (BET) method, yielding a vanadium oxide loading of 1.2 VO_x nm^{-2}.

Raman Spectroscopy. UV Raman spectroscopy was performed using 385 nm wavelength light from a Ti:sapphire solid state laser (Indigo Coherent) for excitation. The fundamental wavelength of 770 nm was converted to 385 nm via a LiB_3O_5 crystal. A triple-stage spectrograph (Princeton Instruments, TriVista 555) and a charge-coupled device (CCD, 2048×512 pixels) camera were employed to disperse and detect the scattered Raman radiation. The spectral resolution of the spectrometer was approximately 1 cm^{-1}. Sample damage was avoided by using a low laser power of 3.8 mW as measured at the sample position and by continuously moving the sample. UV Raman data analysis included cosmic ray removal and background subtraction. Raman spectra at 515 nm wavelength excitation were taken employing an argon ion laser (515 nm, Melles Griot). The spectrometer (Kaiser Optical, HL5R) was combined with an electronically cooled CCD detector (256×1024 pixels). The spectrometer's resolution was 5 cm^{-1} and the wavelength stability was better than 0.5 cm^{-1}. The laser power was adjusted to 1.5 mW as measured at the sample position. Analysis of the Raman data included cosmic ray removal and auto new dark correction. For the Raman experiments 0.15–0.2 g of sample was filled in a CCR1000 reactor (Linkam Scientific Instruments) equipped with a CaF_2 window (Korth Kristalle GmbH).

Diffuse Reflectance UV-Vis Spectroscopy. Diffuse reflectance (DR) UV-Vis spectra were recorded on a UV-Vis spectrometer (Jasco V-770). Approximately 0.06 g of sample was filled in a reaction cell (HVC-MRA-5, Harrick Scientific). Dehydrated magnesium oxide served as a white standard. Optical absorption edges were determined from Tauc plots of $(F(R_\infty)h\nu)^{1/n}$ versus $h\nu$ with $n = 2$.

Catalytic Testing. Catalytic testing was performed in the CCR1000 reactor using 0.15–0.2 g of sample. The samples were first dehydrated at approximately 500 °C for at least 1 h at oxidative conditions (8% O_2, 92% N_2; 50 mL_n min^{-1}). After the sample had cooled down to 73 °C, ethanol (Sigma Aldrich, liquid, ≥99.8% (GC)) was added to the O_2/N_2 stream by bubbling the gas through a saturator cooled to –6 °C. Based on the Antoine equation, the

reaction-gas composition consisted of approximately 1% ethanol, 8% O_2, and 91% N_2. The temperature was raised every 45 min by approximately 9 °C. The gas phase was continuously monitored by Fourier transform IR (FTIR) spectroscopy using a Vertex 70 spectrometer (Bruker) equipped with a RT-DLaTGS (room-temperature deuterated L-alanine-doped triglycine sulfate) detector. Conversion and selectivity were calculated on the basis of FTIR gas-phase analysis.

***Operando* Experiments**. *Operando* Raman and *operando* DR UV-Vis spectra were recorded during reaction conditions at 100 °C. Owing to the low penetration depth of UV radiation, the actual temperature at the surface of the sample was taken into account. The vertical temperature gradient of ceria in the sample holder was determined to be approximately 8 °C. For characterization prior to *operando* experiments, DR UV-Vis and Raman spectra were recorded after dehydration at 100 °C.

3. Results and Discussion

Figure 1 depicts the catalytic performance of a 1.2 VO_x/CeO_2 catalyst in ethanol ODH in comparison to that of the bare support at temperatures between 70 and 150 °C. Out of a series of variously loaded VO_x samples, we chose this loading for a detailed mechanistic study because of the dispersed nature of the surface vanadia species (as evaluated based on visible Raman spectra), which enabled a more direct comparison with the results of previous theoretical calculations. Bare ceria is known for its catalytic activity in ethanol ODH and conversions of <10% have previously been reported at temperatures below 138 °C, in agreement with our results.[28] However, as shown by Figure 1, impregnation of ceria with vanadia leads to a strong increase in conversion. Besides acetaldehyde, the formation of CO_2 and water as well as small amounts of CO is observed. For bare ceria, the selectivities towards acetaldehyde constantly decrease with increasing temperature, while the VO_x/CeO_2 catalyst exhibits a maximum at

around 100 °C. At this temperature, the conversion is 9.5±0.0%, while the selectivity towards acetaldehyde is 85.3±0.6%. To explore the detailed relation between activity and structure for the VO_x/CeO_2 catalyst, a reaction temperature of 100 °C was chosen for the *operando* experiments described below. Please note that vanadia deposited on silica, as a representative of an inactive support material, shows hardly any ethanol conversion below 100 °C,[26] suggesting the presence of a synergetic effect of the VO_x/ceria system, thus exhibiting a total catalytic activity exceeding that of the individual participants.

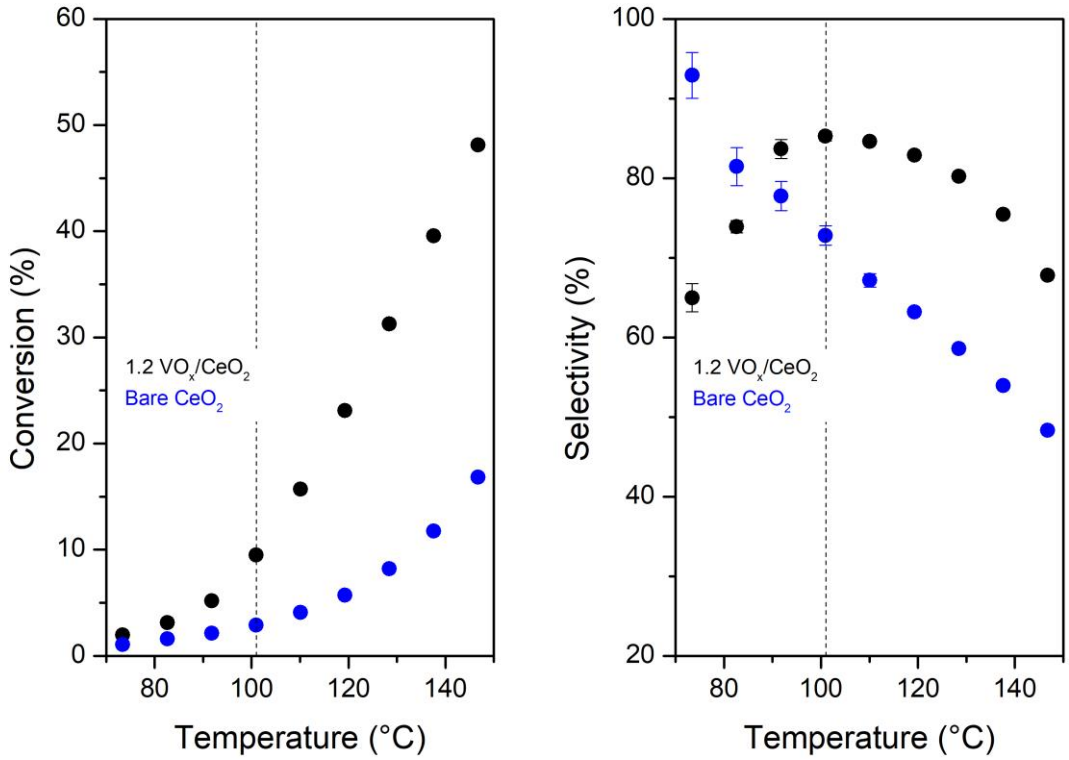

Figure 1. Catalytic performance of 1.2 VO_x/CeO_2 (black) as compared to bare CeO_2 (blue) in the ODH of ethanol (gas composition: 1% EtOH, 8% O_2, 91% N_2; total gas flow: 50 mL_n /min). **Left:** Ethanol conversion as a function of temperature. **Right:** Selectivity towards acetaldehyde as a function of temperature. The dashed lines indicate the temperature chosen for the *operando* experiments.

Figure 2 depicts the DR UV-Vis spectrum of the 1.2 VO_x/CeO_2 catalyst under dehydrated conditions at 100 °C. The UV-Vis spectrum is dominated by the strong self-absorption of ceria below 400 nm (see Figure S1), in agreement with the literature.[25] The maximum at around 265 nm as well as the shoulder at around 330 nm originate from band gap absorption (O 2p(filled) → Ce 4f(empty) transitions).[29] These intense ceria bulk features cover vanadia absorption features arising from ligand-to-metal charge transfer (LMCT) that are usually observed below 300 nm.[30] In contrast to the UV, in the visible region the absorption behavior is dominated by the vanadia-related LMCT features due to oligomeric species and/or 2D aggregates (see inset).[1,30] In the UV-Vis spectrum the excitation wavelengths (385 and 515 nm) used for the Raman experiments are marked; the latter were chosen to enable a selective (resonance) enhancement of ceria- and vanadia-related vibrational features, respectively. In fact, with excitation at 385 nm wavelength, ceria absorption greatly exceeds that of vanadia, thus allowing the dedicated monitoring of ceria surface and bulk modes. On the other hand, with excitation at 515 nm, vanadia-related modes experience more enhancement (compared to 385 nm), enabling the observation of both ceria- and vanadia-related modes. Consequently, our multi-wavelength Raman approach gives access to complementary information about the VO_x/CeO_2 system.

It should be mentioned that originally the Raman spectroscopic characterization included the use of four different laser excitation wavelengths, i.e., 257, 385, 515, and 633 nm. However, as shown in Figure S2, the spectroscopic information obtained from excitation at 257 nm wavelength (as compared to 385 nm) was limited owing to sample absorption, and excitation at 633 nm did not provide any additional information (in comparison to 515 nm).

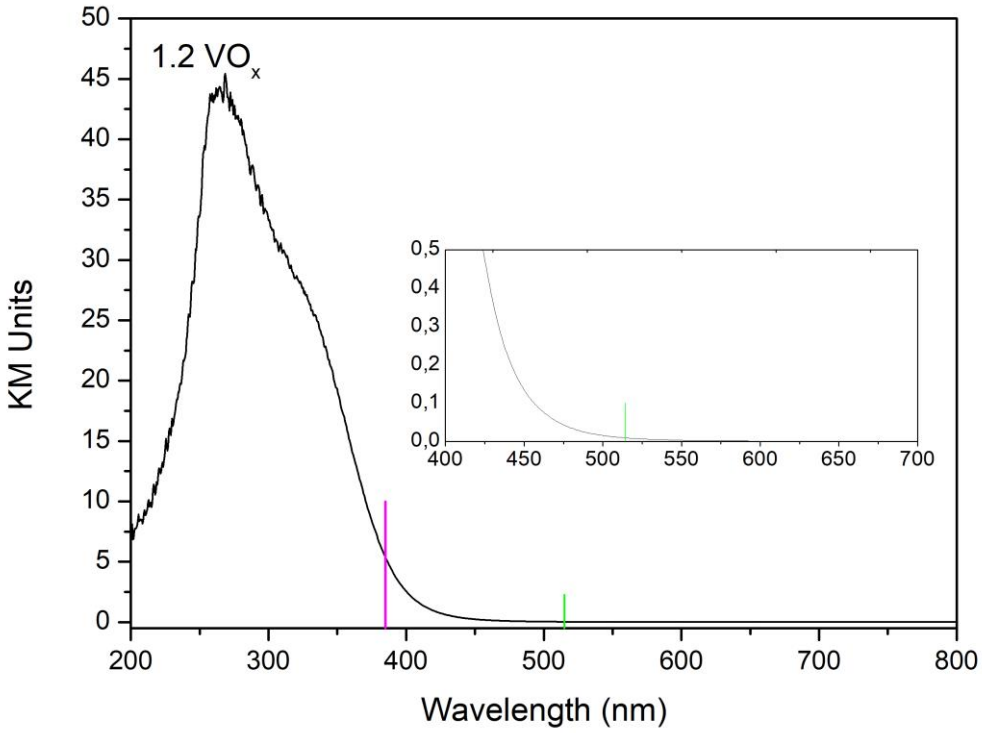

Figure 2. In situ DR UV-Vis spectrum of the 1.2 VO_x/CeO_2 catalyst recorded in 8% O_2/92% N_2 flow at 100 °C. The excitation wavelengths (385 and 515 nm) used for the Raman experiments are marked. The insets give an enlarged view of the visible region of the spectrum.

Figure 3 depicts Raman spectra of the 1.2 VO_x/CeO_2 catalyst for excitation at 385 nm (magenta) and 515 nm (green) wavelengths under dehydrated conditions at 100 °C. Spectra have been normalized to the strongest Raman feature at 465 cm^{-1} (F_{2g} band) and offset for clarity. Enlarging the spectral region 800–1100 cm^{-1} of the 515 nm spectrum (see inset) makes the vanadyl (V=O) stretching band at around 1015 cm^{-1} clearly visible. Detailed analysis reveals that the V=O Raman band consists of (at least) three contributions, which have previously been associated with dimers (~1015 cm^{-1}), trimers (~1030 cm^{-1}), and oligomers (~1040 cm^{-1}).[10,25] Consistent with the Raman spectroscopic findings, the absorption edge energy was determined as 2.95 eV based on UV-Vis analysis, corresponding to an average of 2.5–3 V-O-V bonds per vanadia species.[30]

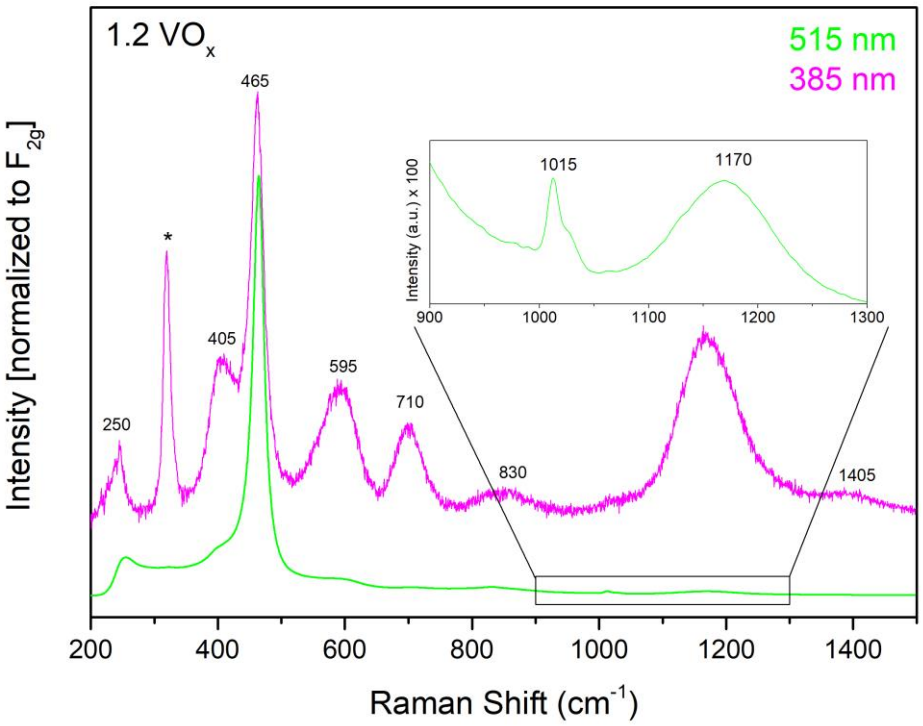

Figure 3. In situ Raman spectra recorded at 385 nm (magenta) and 515 nm (green) wavelength laser excitation. Spectra have been normalized to the F_{2g} band at 465 cm^{-1} and offset for clarity. The artifact (marked with an asterisk) at 320 cm^{-1} is due to the CaF_2 window of the reaction cell. The insets give an enlarged view of the 515 nm spectrum in the range 800–1100 cm^{-1}.

With 385 nm wavelength excitation, besides the characteristic and well-known ceria bulk features at 465 cm^{-1} (F_{2g} band) and 1170 cm^{-1} (2LO),[31] major Raman bands are observed at 250, 405, 595, 710, and 830 cm^{-1}. The features at 250 and 405 cm^{-1} have recently been assigned to longitudinal and transversal surface vibrations of topmost Ce-O bonds, respectively, while a contribution of the bulk TA to the 250 cm^{-1} feature cannot be excluded, as discussed previously in detail.[31] The broad contribution at around 595 cm^{-1} is attributed to bulk oxygen vacancies in the vicinity of Ce^{3+} ions, i.e., $Ce^{3+}O_7V_O^{\bullet\bullet}$, based on DFT calculations.[31] Likewise, a shoulder at around 550 cm^{-1} has previously been assigned to oxygen vacancies further away

from Ce^{3+} ions.[31] The Raman band at 710 cm^{-1} is absent for bare ceria, and increases in intensity with increasing vanadium loading (see Figure S3). This behavior is consistent with V-O-Ce interface vibrations, in agreement with the literature.[25] Interestingly, we observe a weak broad band at around 1405 cm^{-1}, i.e., at almost twice the frequency of this feature, which, to the best of our knowledge, has not been reported previously. Owing to the observed band position and its broadening as compared to the band at 710 cm^{-1}, we propose the 1405 cm^{-1} band to be an overtone of the V-O-Ce vibration. This assignment is further supported by the fact that both features behave similarly in the presence/absence of vanadia (see Figure S3). Finally, for both excitation wavelengths, a Raman band at around 830 cm^{-1} was observed, which has previously been attributed to the O-O stretching vibration of molecular oxygen adsorbed onto a surface oxygen vacancy of ceria forming a peroxide species.[25,27,31,32]

Figure 4 shows the DR UV-Vis spectra of the 1.2 VO_x/CeO_2 catalyst under oxidative (in situ, 8% O_2 / 92% N_2) and reactive (*operando*, 1% EtOH / 8% O_2 / 91% N_2) conditions at 100 °C. The spectra of the vanadia-loaded and bare ceria sample are almost identical in shape and show only slight changes under reaction conditions (see Figure S4 for corresponding spectra of bare ceria). In the UV region, a rather uniform decrease in absorption is observed, which may originate from slightly different reflectance conditions when switching to reactive conditions. In contrast, as shown in the inset, in the visible region a small and broad absorption feature appears under reaction conditions, which shows a more pronounced increase when vanadia is present (see Figure S5). Owing to the overall intensity decrease below 400 nm, we can rule out that this band originates from an off-set or tailing of the main absorption features. As the new band appears not only for VO_x/ceria but also for bare ceria, it may be associated with ceria reduction under reaction conditions, which is known to give rise to an absorption band at around 500 nm.[31,33,34] Notably, the presence of vanadia leads to an increase in the extent of ceria reduction, in good agreement with the Raman results discussed below. Based on the behavior of the bare ceria support, we consider a contribution from d-d transitions of reduced

vanadia to be unlikely, consistent with the results of theoretical calculations predicting the stabilization of surface vanadia species in a +5 oxidation state by the ceria support.[7,10]

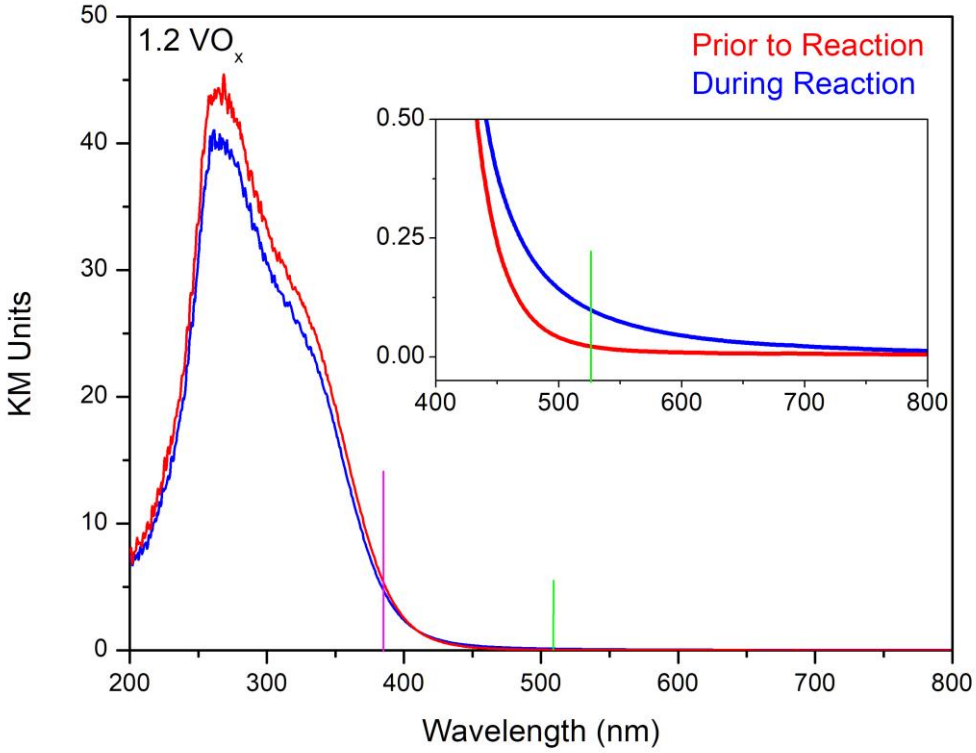

Figure 4. DR UV-Vis spectra of the 1.2 VO_x/CeO_2 catalyst prior to (red) and during (blue) ethanol ODH recorded at 100 °C at a total flow rate of 50 mL_n /min. The feed during in situ conditions consisted of 8% O_2 / 92% N_2; the feed during *operando* conditions consisted of 1% EtOH / 8% O_2 / 91% N_2. The excitation wavelengths (385 nm, 515 nm) used for the Raman experiments are marked. The inset gives an enlarged view of the spectra at longer wavelengths.

Figures 5 and 6 depict the wavelength-dependent Raman spectra of the 1.2 VO_x/CeO_2 catalyst as compared to the bare support under oxidative (in situ, 8% O_2 / 92% N_2) and reactive (*operando*, 1% EtOH / 8% O_2 / 91% N_2) conditions at 100 °C. Spectra recorded excitation at 385 nm wavelength (see Figure 5) display ceria, interface, and oxygen adsorbate features, whereas 515 nm spectra (see Figure 6) cover vanadyl, C-H, and O-H stretching vibrations.

Upon switching from oxidative to reactive conditions, the 385 nm Raman spectra in Figure 5 show a number of noticeable changes: First, a strong decrease of surface phonon bands originating from top-most Ce-O units is observed for VO_x/CeO_2 and bare ceria, continuing until the disappearance of the signal at 405 cm^{-1} (see Figure S6). This behavior results from a reduction of surface ceria, i.e., the consumption of surface lattice oxygen.[29,31] In both cases, subsurface ceria undergoes a reduction, as evidenced by the small but reproducible redshift of the F_{2g} band (see inset),[29,31] which is more prominent for VO_x/CeO_2, and fully consistent with the UV-Vis results discussed above. Second, the interface V-O-Ce band at around 710 cm^{-1} exhibits a blueshift and a significant intensity decrease, indicating the modification and consumption of V-O-Ce linkages. In addition, the peroxide-related feature at around 830 cm^{-1} undergoes a redshift and narrowing, indicative of a transformation of aggregated into more isolated peroxide species according to recent DFT calculations.[31,35] As discussed previously in detail,[31,35] the presence of peroxide species can be considered as an indicator for surface oxygen vacancies. Thus, the observed peroxide dynamics are interpreted as a redistribution of oxygen vacancies in VO_x/CeO_2 and bare ceria upon switching to reaction conditions.

Complementary information was obtained by Raman spectra using 515 nm wavelength excitation, as shown in Figure 6. Upon switching from oxidative to reactive conditions, the vanadia-related features at around 1015 and 1030 cm^{-1} experience a substantial loss in intensity and a downward shift to 1000 cm^{-1}. We attribute this behavior to the coordination of ethanol and/or water to the vanadia structure, leading to a lengthening of the V=O bond.[25,36–41] Consistent with these findings, previous studies had reported the presence of Raman features ≤1000 cm^{-1} for supported vanadia exposed to water or alcohols.[25,36–41] In this context, Raman studies on VO_x/CeO_2 reported a shift of the terminal V=O bond under hydrated conditions.[42] For example, for 1% V_2O_5/CeO_2 (3% V_2O_5/CeO_2), V=O redshifts of 15 cm^{-1} (9 cm^{-1}) were detected in the presence of water vapor for VO_x/CeO_2 at 170 °C, which was explained by hydrogen-bonded surface VO_x species solvated by water molecules.[43] Considering the lower

temperature applied in the present study, 100 °C, the presence of larger amounts of water or alcohols and, as a consequence, stronger V=O redshifts are expected.

The effect of moisture on the V=O stretching frequency was also confirmed by DFT calculations performed for VO_x/titania with a loading of 0.84 VO_x nm^{-2},[44,45] which leads to the conclusion that the experimentally observed redshift may result from hydrogen bonding between the vanadyl bond and surface hydroxyl group (V-OH, Ti-OH) or water molecules. Depending on the degree of hydration, the presence of water is considered responsible for the hydrolysis process stabilizing monomers and breaking V-O-M bonds. Secondly, V-OH bonds are formed. Further hydration may then lead to molecular water at the surface, and to the formation of completely solvated $OV(OH)_3$ species, which do not contain any bridging V-O-M bonds and are stabilized to the metal surface by hydrogen bonds. At higher vanadium loading (3.37 VO_x nm^{-2}) two competitive processes may occur: oligomerization, i.e., formation of V-O-V bonds, and solvation, i.e., formation of vanadium ions with penta- and hexa-coordination.[44] Our DR UV-Vis spectroscopic results (see Figure 4) do not indicate oligomerization processes and/or significant structural changes. In fact, the value of the absorption edge energy of 1.2 VO_x/CeO_2 of 2.95 eV does not change upon exposure to reaction conditions, indicating no change in the number of V-O-V bonds. Besides, no additional absorption bands, which would suggest an increase in the coordination of the vanadium ions, are observed. According to Figure 5, the exposure to reaction conditions leads to a substantial (50%) loss of the V-O-Ce band intensity. However, there are still a sufficient number of V-O-Ce bonds to attach all vanadia species to the surface of the ceria support, based on the commonly accepted structure of ceria-supported vanadia,[46,47] according to which, prior to reaction each vanadium center is anchored to the support by at least three V-O-Ce bonds for monomeric structures and, accordingly, by at least two V-O-Ce bonds for dimeric structures. We therefore attribute the observed redshift of the V=O band to the coordination of ethanol and/or water to the surface vanadia structure, in agreement with a lengthening of the bond. As a result of the coordination,

the local structure of the vanadium center is expected to undergo changes, which may give rise to changes in the orientation of the V=O bonds, leading to a decrease in Raman intensity, similarly to what has previously been discussed in the context of IR spectra.[22] However, in order to clarify the V=O intensity changes associated with the exposure to reaction conditions, it will be necessary to perform theoretical calculations in the future.

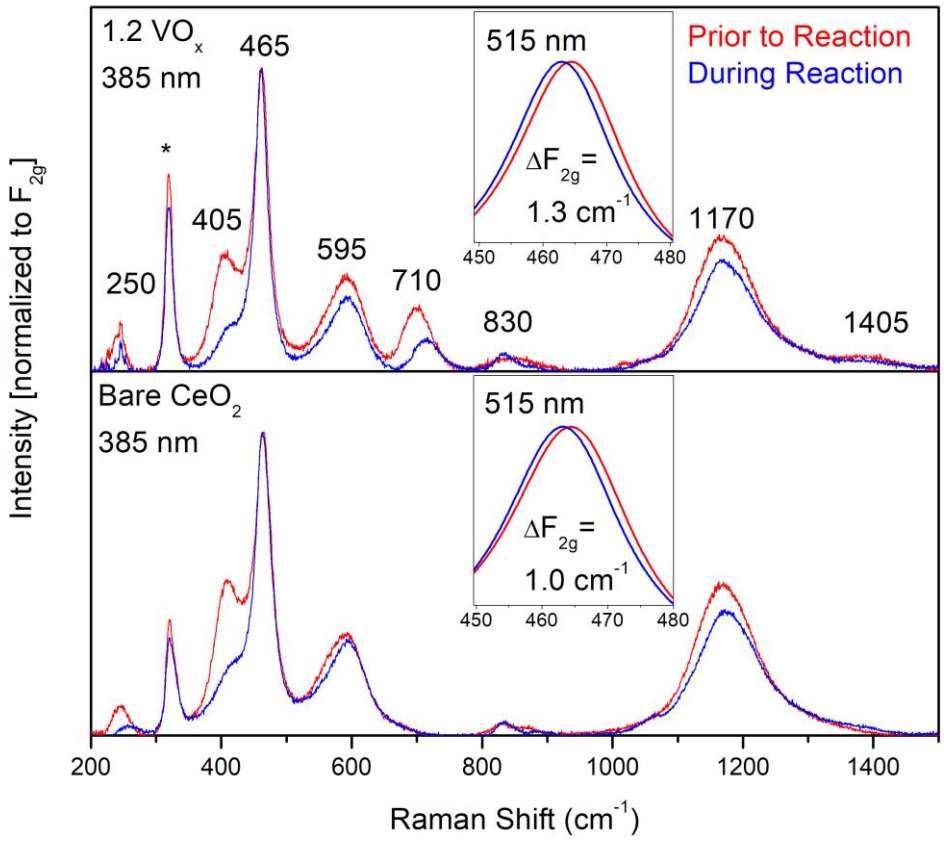

Figure 5. 385 nm Raman spectra of the 1.2 VO_x/CeO_2 catalyst (top panel) as compared to bare ceria (bottom panel) prior to (red) and during (blue) ethanol ODH recorded at 100 °C at a total flow rate of 50 mL_n /min. The feed during in situ conditions consisted of 8% O_2 / 92% N_2; the feed during *operando* conditions consisted of 1% EtOH / 8% O_2 / 91% N_2. Insets show the changes in F_{2g} position when switching to operando conditions (515 nm). Spectra have been normalized to the F_{2g} band.

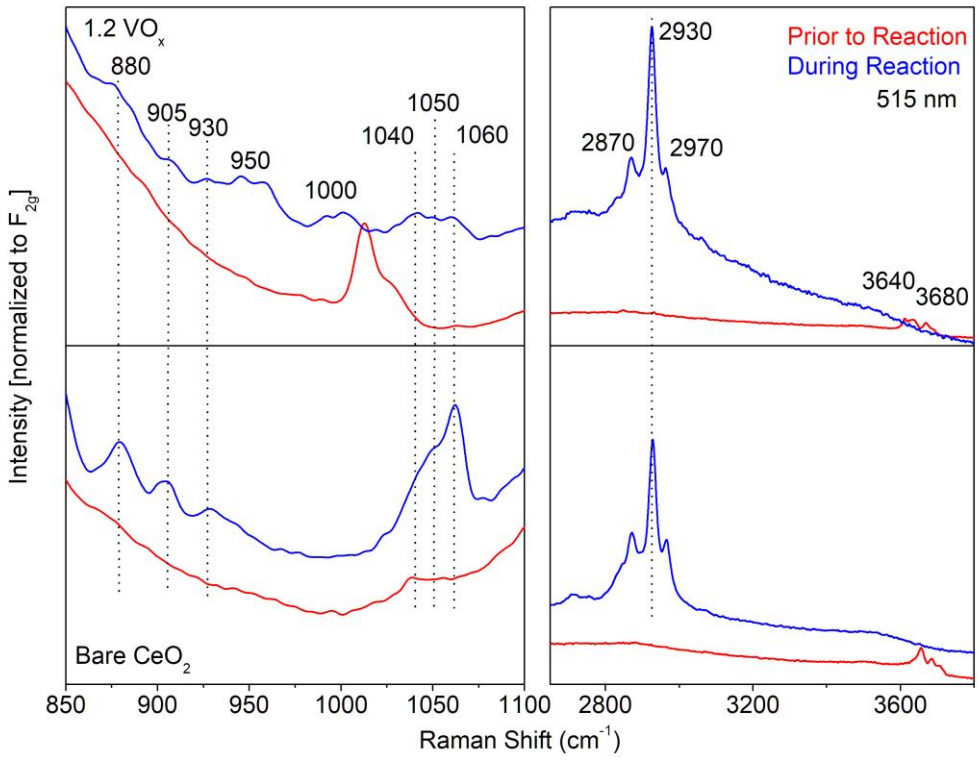

Figure 6. 515 nm Raman spectra of the 1.2 VO_x/CeO_2 catalyst (top panel) as compared to bare ceria (bottom panel) prior to (red) and during (blue) ethanol ODH recorded at 100 °C at a total flow rate of 50 mL_n /min. The feed during in situ conditions consisted of 8% O_2 / 92% N_2; the feed during *operando* conditions consisted of 1% EtOH / 8% O_2 / 91% N_2. Spectra have been normalized to the F_{2g} band and offset for clarity.

As can be seen on the right of Figure 6, in the C-H stretching region, exposure to reaction conditions results in the adsorption of ethanol. The vibrational signature observed for the VO_x/CeO_2 sample strongly resembles that of bare ceria. Detailed analysis reveals the presence of Raman bands at around 2870, 2930, and 2970 cm^{-1}, which can be assigned to $\nu_s(CH_2)$, $\nu_s(CH_3)$, and $\nu_{as}(CH_3)$ modes, respectively, in agreement with the literature.[48–50] According to previous studies,[51] ethanol adsorption on $CeO_2(111)$ results in the formation of ethoxy species at temperatures <550 K. We therefore attribute the observed C-H stretching

vibrations to the formation of ethoxy species that are predominantly adsorbed on the ceria surface.

The left panel of Figure 6 shows that, apart from the dynamics of the V=O band, a series of new Raman bands appears at around 880, 905, 930, 1040, 1050, and 1060 cm^{-1} under reaction conditions for 1.2 VO_x/CeO_2 (top of Figure 6) and bare ceria (bottom of Figure 6). In addition, there is a broad feature at around 950 cm^{-1}, which is especially prominent for the VO_x/CeO_2 sample, indicating its relation to the presence of vanadium, as discussed below. The Raman bands at around 1040, 1050, and 1060 cm^{-1} can be assigned to C-O stretching modes of ethoxy species, in agreement with previous IR and Raman spectroscopic studies.[50,52–55] The vibrations at 880, 905, 930, and 950 cm^{-1} are located in the range of C-C stretching modes and suggest the presence of different ethoxy species. Previously, IR bands detected at 1050 and 885 cm^{-1} after ethanol exposure to CeO_2(111) were assigned to C-O and C-C stretching vibrations of bidentate ethoxide or ethoxide in an oxygen vacancy, and bands at 1096 and 905 cm^{-1} to the corresponding vibrations of monodentate species.[52,53] The joint decrease of the intensity of the C-C and C-O stretching modes for the VO_x/CeO_2 sample in comparison to bare ceria (and also as a function of the vanadium loading as shown in Figure S7) points to a reduction of the number of ethoxy species adsorbed at the ceria surface. Such a behavior is expected based on the coverage of the ceria support by vanadia (~12% of vanadia monolayer at 10 V/nm^2). On the other hand, comparison of the Raman spectrum of VO_x/CeO_2 with that of bare ceria under reaction conditions reveals the presence of a vanadium-related band at around 950 cm^{-1}, in addition to the 1000 cm^{-1} feature discussed above. In previous *operando* Raman studies on ethanol ODH over VO_x/SiO_2 catalysts, bands at 922 and 1056 cm^{-1} have been assigned to C-C and C-O stretching vibrations, respectively, of ethoxy directly attached to vanadium.[26] This assignment was based on wavelength-dependent studies showing a resonance effect of the C-C-O vibration triggered by the VO_4 oscillator, in agreement with previous studies on titanium alkoxides.[56] Thus, we may attribute the Raman feature at around 950 cm^{-1} to the C-C vibration

of ethoxy bound to vanadium. However, as there is some overlap with the 930 cm^{-1} ceria feature, a contribution of ceria-bound ethoxy cannot be excluded. The corresponding C-O vibration of V-bound ethoxy is expected to be part of the C-O-related feature between 1030 and 1070 cm^{-1}. The presence of ethoxy attached to vanadium is supported by the C-H stretching region, which shows an intensity increase (see e.g. the 2930 cm^{-1} band in Figure 6), indicating an increase in the total amount of adsorbed ethoxy, despite the reduction of ceria-bound ethoxy for vanadia-containing catalysts.

Finally, as shown in the right panel of Figure 6, switching to reaction conditions results in the complete disappearance of hydroxyl groups at 3640 and 3680 cm^{-1} and the appearance of a broad OH-related band between 3300 and 3700 cm^{-1} for both VO_x/CeO_2 and bare ceria. The loss of sharp features may be associated with hydrogen bonding interactions of OH groups with adsorbed ethoxy species and/or water, which is formed as a reaction product.[57] A summary of observed Raman bonds and their assignments is given in Table 1.

Table 1. Summary of Raman bands for bare CeO_2 and 1.2 VO_x/CeO_2, as observed in this work.

Position (cm^{-1})	Assignment		References
250	Ce-O longitudinal stretch, 2TA	CeO_2(111) surface, CeO_2(111) bulk	31
405	Ce-O transversal stretch	CeO_2(111) surface	31
465	F_{2g}	CeO_2(111) bulk	27,31
595	Oxygen vacancies	Reduced CeO_{2-x} bulk	31
710	V-O-Ce	Interface	25
830	O-O	Peroxides	25,27,31,32
880	C-C	Ethoxy	52
905	C-C	Ethoxy	52

930	C-C	Ethoxy	this work
950	C-C	Ethoxy	this work
1000	V=O	Vanadyl coordinated with water/ethanol	[43]
1015	V=O	Dimer	[10,25]
1030	V=O	Trimer/Oligomers	[10,25]
1040	C-O	Ethoxy	this work
1050	C-O	Ethoxy	[52,53]
1060	C-O	Ethoxy	this work
1170	2LO	CeO_2(111) bulk	[27,31]
1405	2V-O-Ce	Interface (overtone)	this work
2870	$\nu_s(CH_2)$	Ethoxy	[52]
2930	$\nu_s(CH_3)$	Ethoxy	[52]
2970	$\nu_{as}(CH_3)$	Ethoxy	[52]
3640	O-H (II*-B)	Doubly bridging hydroxyl group on reduced ceria	[27,58]
3680	O-H (II*-A)	Doubly bridging hydroxyl group on reduced ceria	[27,58]

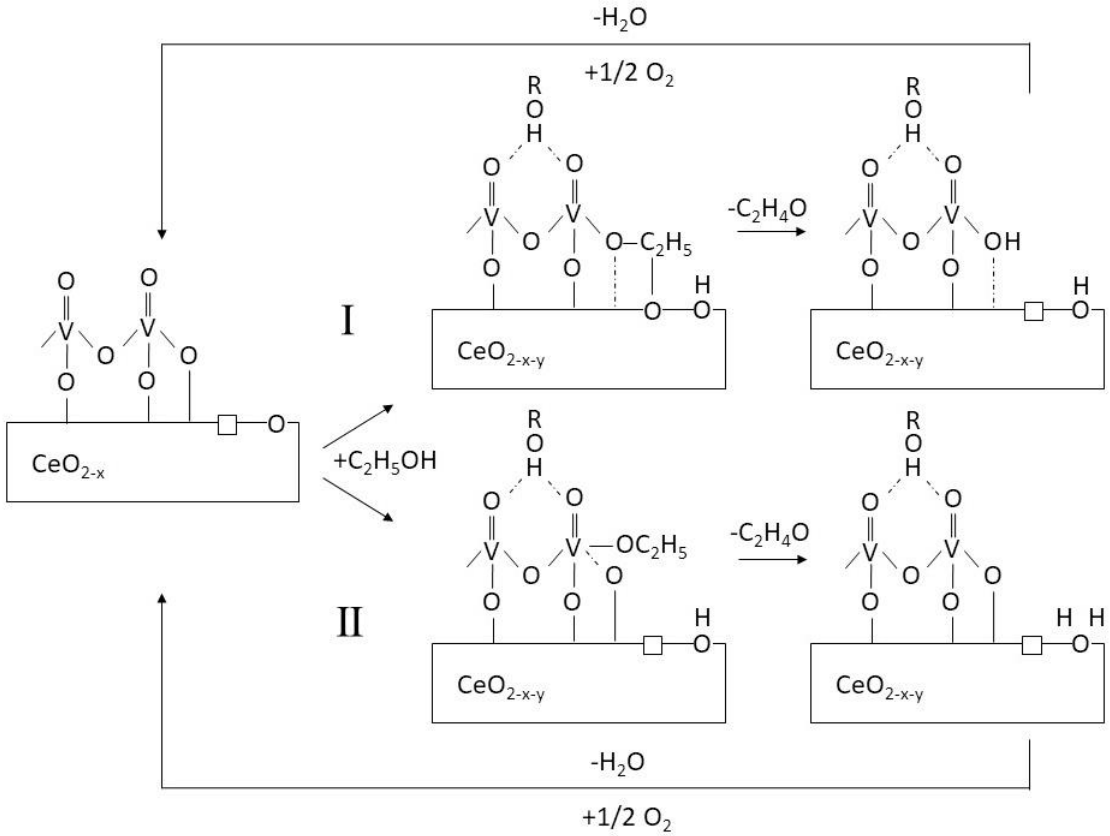

Figure 7. Proposed reaction mechanisms for the ODH of ethanol over VO_x/CeO_2 catalysts.

Based on our spectroscopic findings, we propose the following reaction mechanisms for ethanol ODH over VO_x/CeO_2 catalysts and bare ceria (see Figure 7): Pathway I involves the chemisorption of ethanol on the ceria surface as ethoxy species, as shown by the presence of C-C, C-O, and C-H stretching vibrations, accompanied by hydrogen transfer to lattice oxygen, as indicated by the disappearance of the surface phonon signal at 405 cm^{-1} (see Figure 5, see Figure S6). Besides, a redshift of the F_{2g} mode is observed (see Figure 5), which can be associated with the formation of oxygen vacancies in the ceria subsurface (see CeO_{2-x-y} in Figure 7),[31,34] indicating the transfer of oxygen to the surface. As not only top ceria atoms but also subsurface ceria undergo reduction, we conclude that the support serves as an oxygen buffer, being able to release stored oxygen. In comparison, for bare ceria, exposure to reaction conditions induces ceria-related spectral changes similar to those for the loaded sample. In this case, the observed conversion to acetaldehyde may then proceed by another hydrogen transfer

to a hydroxyl group, leading to water formation, as suggested by the changes in the O-H stretching region. For the vanadium-loaded sample, however, additional vanadia-related spectral changes are observed, e.g., a blueshift of the V-O-Ce interface bond (see Figure 5, top panel). We attribute the observed shift to ethoxy adsorbed in the vicinity of surface vanadia modifying the interface bond (see Figure 7) and thereby facilitating a subsequent hydrogen transfer to V-O-Ce, consistent with predictions from theory.[22] The structural changes of the surface vanadia species upon exposure to ethanol ODH conditions are attributed to the coordination of EtOH and/or water. There is no indication from experiment of significant vanadia reduction, in agreement with the DFT literature.[22,24] Thus vanadia appears to play a coordinative role rather than that of a redox system.

Pathway II involves the adsorption of ethanol at the vanadium center by breaking a V-O-Ce interface bond (see Figure 7), as evidenced by the decrease in V-O-Ce intensity (see Figure 5, top panel). As a result, a vanadium-bound ethoxy species is formed, as suggested by the appearance of the C-C stretching feature at around 950 cm^{-1} (see Figure 6, top panel). The process of ethoxy formation from adsorbed ethanol is accompanied by hydrogen transfer to lattice oxygen, as described above in the context of pathway I. The subsequent conversion to acetaldehyde may then involve another hydrogen transfer to lattice oxygen or to a hydroxyl group, leading to water formation, as suggested by the changes in the O-H stretching region.

A further aspect of the support participation in the ethanol ODH reaction was elucidated by switching experiments, in which the gas phase was cycled between oxidative (O_2/N_2) and reactive ($EtOH/O_2/N_2$) conditions, and the F_{2g} position was monitored as an indicator for the ceria stoichiometry (see Table S1). The F_{2g} red-shift upon switching from oxidative to reactive conditions was followed by a F_{2g} blue-shift when retuning to oxidative conditions, thus clearly indicating the consumption and replenishment of ceria subsurface oxygen. The full recovery to the initial F_{2g} position (prior reaction) requires heating to elevated temperatures, which may be attributed to the removal of residual adsorbates hindering the oxygen transfer to the ceria

subsurface. For differently loaded catalysts (0.6 VO_x/CeO_2, 1.2 VO_x/CeO_2), we observed similar F_{2g} shifts, which were significantly larger as in case of bare ceria. Thus, while the presence of vanadia has a marked effect on the oxygen dynamics, increasing the vanadium loading does not necessarily lead to a larger buffering effect.

Figure 1 shows the remarkable activity of the 1.2 VO_x/CeO_2 catalyst for ethanol ODH at low temperatures. The comparison with the conversion values of bare ceria and vanadia (supported on silica) suggests the presence of a cooperative effect of the vanadia/ceria system, thus exhibiting a total catalytic activity exceeding that of the individual participants. In fact, vanadia deposited on silica as an inactive support shows hardly any conversion below 100 °C.[26] Our spectroscopic findings may offer an explanation for the observed catalytic behavior: Pathway I involves the adsorption of ethanol on the ceria surface leading to ethoxy formation. The subsequent hydrogen transfer is crucial as it is considered the rate-determining step of the reaction. In the presence of vanadia the hydrogen transfer may be strongly facilitated by formation of a V-O---H-C_2H_4O transfer site[22] followed by acetaldehyde formation using lattice oxygen, thus following a scenario that has not been reported for silica-supported vanadia.

4. Conclusion

Summarizing, we have provided direct spectroscopic evidence for the participation of a ceria support in oxide catalysis. As demonstrated for a VO_x/CeO_2 catalyst during ethanol ODH, ceria lattice oxygen, the V-O-Ce interface, as well as ceria subsurface oxygen, are shown to be directly involved in the reaction, underlining the active participation of the support in the redox process. We have developed an experimental basis for a detailed understanding of the support participation, which we consider to be of more general importance in oxide catalysis.

From our study it is apparent that a combination of *operando* techniques is necessary to gain insight into the complex interplay of the different oxides under working conditions,

regarding structural as well as redox properties. In particular, as illustrated here for VO_x/CeO_2, in order to be able to untangle the dynamics of ceria from those of vanadia during catalysis, we employed *operando* wavelength-selective Raman spectroscopy, in addition to *operando* UV-Vis spectroscopy. This approach had not been applied in this context before, despite its potential to enable selective excitation of the vibrational features of the support and the deposited phase. In the case of VO_x/CeO_2 catalysts, the use excitation at 385 nm wavelength for the ceria support and 515 nm for the vanadia phase is demonstrated to be an efficient combination, and we expect also other supported oxide catalysts to be accessible by adjusting the Raman excitation wavelengths.

Based on our findings from combined *operando* spectroscopy we have proposed a mechanism for the ethanol ODH reaction over VO_x/CeO_2 catalysts. Clearly extending previous work, this mechanism explicitly takes into account the new experimental results from this study, including the various facets of the oxygen support dynamics. It therefore allows for direct comparison with previous mechanistic proposals based on DFT calculations on methanol ODH. Importantly, both our experiments and the theoretical studies demonstrate that the V-O-Ce interface plays a crucial role in facilitating the ODH reaction and that vanadium keeps its +5 oxidation state under reaction conditions, i.e., that vanadium is not participating as a redox system. An important future task will be to explore the generalizability of these findings and to further develop our approach towards kinetic experiments,[59]

It is an exciting prospect to transfer the above experimental approach to other supported oxides and reactions, such as propane ODH, which is of relevance for technical applications. Regarding the substrate (e.g. propane), we do not expect any limitations from the experimental side as the applicability of our approach is largely determined by the choice of the catalyst system. With respect to the support material, besides ceria, e.g. titania, as a very common material in oxide catalysis, may be of interest. To study its potential participation, suitable phonon bands, which describe the oxygen dynamics on the surface and/or in the bulk, would

need to be identified first, e.g. by following the procedures recently published for ceria.[31,29] In case of other supported oxides, the optimal choice of the excitation wavelengths for a given support material may depend on the specific UV-Vis absorption properties, but we still expect the general applicability of our Raman approach to a broad range of materials used in oxide catalysis. To this end, knowledge of the UV-Vis absorption properties will strongly facilitate the choice of appropriate Raman excitation wavelengths. Thus, the combination of targeted Raman spectroscopy with UV-Vis spectroscopy will allow an optimal exploitation of spectroscopic information in future applications.

Acknowledgements

The authors acknowledge Silvio Heinschke for performing nitrogen adsorption/desorption experiments, Karl Kopp for technical support, as well as Philipp Waleska, Christian Schilling, and Anastasia Filtschew for fruitful discussions. Patrick Ober thanks the German Academic Scholarship Foundation (Studienstiftung des Deutschen Volkes) for a scholarship. This work was supported by the Deutsche Forschungsgemeinschaft (DFG HE 4515/11-1).

Supporting information

This information is available free of charge on the ACS Publications website.

Additional Raman and UV-Vis spectroscopic data.

References

(1) Beck, B.; Harth, M.; Hamilton, N. G.; Carrero, C.; Uhlrich, J. J.; Trunschke, A.; Shaikhutdinov, S.; Schubert, H.; Freund, H.-J.; Schlögl, R.; Sauer, J.; Schomäcker, R. Partial Oxidation of Ethanol on Vanadia Catalysts on Supporting Oxides with Different Redox Properties Compared to Propane. *J. Catal.* **2012**, *296*, 120–131.

(2) Carrero, C. A.; Schloegl, R.; Wachs, I. E.; Schomaecker, R. Critical Literature Review of the Kinetics for the Oxidative Dehydrogenation of Propane over Well-Defined Supported Vanadium Oxide Catalysts. *ACS Catal.* **2014**, *4*, 3357–3380.

(3) Cavani, F.; Ballarini, N.; Cericola, A. Oxidative Dehydrogenation of Ethane and Propane. *Catal. Today* **2007**, *127*, 113–131.

(4) Cavani, F.; Trifirò, F. The Oxidative Dehydrogenation of Ethane and Propane as an Alternative Way for the Production of Light Olefins. *Catal. Today* **1995**, *24*, 307–313.

(5) Carrero, C. A.; Keturakis, C. J.; Orrego, A.; Schomäcker, R.; Wachs, I. E. Anomalous Reactivity of Supported V_2O_5 Nanoparticles for Propane Oxidative Dehydrogenation. *Dalton Trans.* **2013**, *42*, 12644–12653.

(6) Dinse, A.; Frank, B.; Hess, C.; Habel, D.; Schomäcker, R. Oxidative Dehydrogenation of Propane over Low-Loaded Vanadia Catalysts. *J. Mol. Catal. A: Chem.* **2008**, *289*, 28–37.

(7) Ganduglia-Pirovano, M. V.; Popa, C.; Sauer, J.; Abbott, H.; Uhl, A.; Baron, M.; Stacchiola, D.; Bondarchuk, O.; Shaikhutdinov, S.; Freund, H.-J. Role of Ceria in Oxidative Dehydrogenation on Supported Vanadia Catalysts. *J. Am. Chem. Soc.* **2010**, *132*, 2345–2349.

(8) Bañares, M.A.; Martínez-Huerta, M.V.; Gao, X.; Fierro, J.L.G.; Wachs, I.E. Dynamic Behavior of Supported Vanadia Catalysts in the Selective Oxidation of Ethane. *Catal. Today* **2000**, *61*, 295–301.

(9) Tian, H.; Ross, E. I.; Wachs, I. E. Quantitative Determination of the Speciation of Surface Vanadium Oxides and Their Catalytic Activity. *J. Phys. Chem. B* **2006**, *110*, 9593–9600.

(10) Baron, M.; Abbott, H.; Bondarchuk, O.; Stacchiola, D.; Uhl, A.; Shaikhutdinov, S.; Freund, H.-J.; Popa, C.; Ganduglia-Pirovano, M. V.; Sauer, J. Resolving the Atomic Structure of Vanadia Monolayer Catalysts. *Angew. Chem. Int. Ed.* **2009**, *48*, 8006–8009.

(11) Martínez-Huerta, M. V.; Deo, G.; Fierro, J. L. G.; Bañares, M. A. Operando Raman-GC Study on the Structure−Activity Relationships in V^{5+}/CeO_2 Catalyst for Ethane Oxidative Dehydrogenation. *J. Phys. Chem. C* **2008**, *112*, 11441–11447.

(12) Iglesias-Juez, A.; Martínez-Huerta, M. V.; Rojas-García, E.; Jehng, J.-M.; Bañares, M. A. On the Nature of the Unusual Redox Cycle at the Vanadia Ceria Interface. *J. Phys. Chem. C* **2018**, *122*, 1197–1205.

(13) Martínez-Huerta, M. V. Nature of the Vanadia–Ceria Interface in V^{5+}/CeO_2 Catalysts and its Relevance for the Solid-State Reaction Toward $CeVO_4$ and Catalytic Properties. *J. Catal.* **2004**, *225*, 240–248.

(14) Martínez-Huerta, M. V.; Deo, G.; Fierro, J. L. G.; Bañares, M. A. Changes in Ceria-Supported Vanadium Oxide Catalysts during the Oxidative Dehydrogenation of Ethane and Temperature-Programmed Treatments. *J. Phys. Chem. C* **2007**, *111*, 18708–18714.

(15) Bosco, M. V.; Bañares, M. A.; Martínez-Huerta, M. V.; Bonivardi, A. L.; Collins, S. E. In Situ FTIR and Raman Study on the Distribution and Reactivity of Surface Vanadia Species in V_2O_5/CeO_2 Catalysts. *J. Mol. Catal. A: Chem.* **2015**, *408*, 75–84.

(16) Daniell, W.; Ponchel, A.; Kuba, S.; Anderle, F.; Weingand, T.; Gregory, D. H.; Knözinger, H. Characterization and Catalytic Behavior of VO_x–CeO_2 Catalysts for the Oxidative Dehydrogenation of Propane. *Top. Catal.* **2002**, *20*, 65–74.

(17) Kropp, T.; Paier, J. Reactions of Methanol with Pristine and Defective Ceria (111) Surfaces. *J. Phys. Chem. C* **2014**, *118*, 23690–23700.

(18) Li, Y.; Wei, Z.; Gao, F.; Kovarik, L.; Baylon, R. A. L.; Peden, C. H. F.; Wang, Y. Effect of Oxygen Defects on the Catalytic Performance of VO_x/CeO_2 Catalysts for Oxidative Dehydrogenation of Methanol. *ACS Catal.* **2015**, *5*, 3006–3012.

(19) Liu, J.; Wu, X.-P.; Zou, S.; Dai, Y.; Xiao, L.; Gong, X.-Q.; Fan, J. Origin of the High Activity of Mesoporous CeO_2 Supported Monomeric VO_x for Low-Temperature Gas-Phase Selective Oxidative Dehydrogenation of Benzyl Alcohol. *J. Phys. Chem. C* **2014**, *118*, 24950–24958.

(20) Penschke, C.; Paier, J.; Sauer, J. Oligomeric Vanadium Oxide Species Supported on the CeO_2 (111) Surface. *J. Phys. Chem. C* **2013**, *117*, 5274–5285.

(21) Abbott, H. L.; Uhl, A.; Baron, M.; Lei, Y.; Meyer, R. J.; Stacchiola, D. J.; Bondarchuk, O.; Shaikhutdinov, S.; Freund, H. J. Relating Methanol Oxidation to the Structure of Ceria-Supported Vanadia Monolayer Catalysts. *J. Catal.* **2010**, *272*, 82–91.

(22) Kropp, T.; Paier, J.; Sauer, J. Support Effect in Oxide Catalysis: Methanol Oxidation on Vanadia/Ceria. *J. Am. Chem. Soc.* **2014**, *136*, 14616–14625.

(23) Kropp, T.; Paier, J.; Sauer, J. Oxidative Dehydrogenation of Methanol at Ceria-Supported Vanadia Oligomers. *J. Catal.* **2017**, *352*, 382–387.

(24) Wu, X.-P.; Gong, X.-Q. Unique Electronic and Structural Effects in Vanadia/Ceria-Catalyzed Reactions. *J. Am. Chem. Soc.* **2015**, *137*, 13228–13231.

(25) Wu, Z.; Rondinone, A. J.; Ivanov, I. N.; Overbury, S. H. Structure of Vanadium Oxide Supported on Ceria by Multiwavelength Raman Spectroscopy. *J. Phys. Chem. C* **2011**, *115*, 25368–25378.

(26) Waleska, P.; Rupp, S.; Hess, C. Operando Multiwavelength and Time-Resolved Raman Spectroscopy. *J. Phys. Chem. C* **2018**, *122*, 3386–3400.

(27) Filtschew, A.; Hofmann, K.; Hess, C. Ceria and Its Defect Structure. *J. Phys. Chem. C* **2016**, *120*, 6694–6703.

(28) Beste, A.; Overbury, S. H. Pathways for Ethanol Dehydrogenation and Dehydration Catalyzed by Ceria (111) and (100) Surfaces. *J. Phys. Chem. C* **2015**, *119*, 2447–2455.

(29) Schilling, C.; Hess, C. Real-Time Observation of the Defect Dynamics in Working Au/CeO_2 Catalysts by Combined Operando Raman/UV–Vis Spectroscopy. *J. Phys. Chem. C* **2018**, *122*, 2909–2917.

(30) Nitsche, D.; Hess, C. Structure of Isolated Vanadia and Titania. *J. Phys. Chem. C* **2016**, *120*, 1025–1037.

(31) Schilling, C.; Hofmann, A.; Hess, C.; Ganduglia-Pirovano, M. V. Raman Spectra of Polycrystalline CeO_2. *J. Phys. Chem. C* **2017**, *121*, 20834–20849.

(32) Pushkarev, V. V.; Kovalchuk, V. I.; d'Itri, J. L. Probing Defect Sites on the CeO_2 Surface with Dioxygen. *J. Phys. Chem. B* **2004**, *108*, 5341–5348.

(33) Laachir, A.; Perrichon, V.; Badri, A.; Lamotte, J.; Catherine, E.; Lavalley, J. C.; El Fallah, J.; Hilaire, L.; Le Normand, F.; Quéméré, E.; Sauvion, G. N.; Touret, O. Reduction of CeO_2 by Hydrogen. Magnetic Susceptibility and Fourier-Transform Infrared, Ultraviolet and X-Ray Photoelectron Spectroscopy Measurements. *J. Chem. Soc., Faraday Trans.* **1991**, *87*, 1601–1609.

(34) Schilling, C.; Hess, C. Elucidating the Role of Support Oxygen in the Water–Gas Shift Reaction over Ceria-Supported Gold Catalysts Using Operando Spectroscopy. *ACS Catal.* **2019**, *9*, 1159–1171.

(35) Schilling, C.; Ganduglia-Pirovano, M. V.; Hess, C. Experimental and Theoretical Study on the Nature of Adsorbed Oxygen Species on Shaped Ceria Nanoparticles. *J. Phys. Chem. Lett.* **2018**, *9*, 6593–6598.

(36) Gao, X.; Bare, S. R.; Weckhuysen, B. M.; Wachs, I. E. In Situ Spectroscopic Investigation of Molecular Structures of Highly Dispersed Vanadium Oxide on Silica under Various Conditions. *J. Phys. Chem. B* **1998**, *102*, 10842–10852.

(37) Abello, L.; Husson, E.; Repelin, Y.; Lucazeau, G. Structural Study of Gels of V_2O_5. *J. Solid State Chem.* **1985**, *56*, 379–389.

(38) Repelin, Y.; Husson, E.; Abello, L.; Lucazeau, G. Structural Study of Gels of V_2O_5. *Spectrochim. Acta A* **1985**, *41*, 993–1003.

(39) Xie, S.; Iglesia, E.; Bell, A. T. Effects of Hydration and Dehydration on the Structure of Silica-Supported Vanadia Species. *Langmuir* **2000**, *16*, 7162–7167.

(40) Hess, C. Characterization of the Synthesis and Reactivity Behavior of Nanostructured Vanadia Model Catalysts Using XPS and Vibrational Spectroscopy. *Surf. Sc.* **2006**, *600*, 3695–3701.

(41) Schraml-Marth, M.; Wokaun, A.; Pohl, M.; Krauss, H.-L. Spectroscopic Investigation of the Structure of Silica-Supported Vanadium Oxide Catalysts at Submonolayer Coverages. *J. Chem. Soc., Faraday Trans.* **1991**, *87*, 2635.

(42) The extent of the V=O redshift was observed to decrease when the amount of adsorbed ethanol was reduced by switching to oxidative conditions, consistent with the other findings and the literature.

(43) Jehng, J.-M.; Deo, G.; Weckhuysen, B. M.; Wachs, I. E. Effect of Water Vapor on the Molecular Structures of Supported Vanadium Oxide Catalysts at Elevated Temperatures. *J. Mol. Catal. A: Chem.* **1996**, *110*, 41–54.

(44) Lewandowska, A. E.; Calatayud, M.; Tielens, F.; Bañares, M. A. Hydration Dynamics for Vanadia/Titania Catalysts at High Loading. *J. Phys. Chem. C* **2013**, *117*, 25535–25544.

(45) Lewandowska, A. E.; Calatayud, M.; Tielens, F.; Bañares, M. A. Dynamics of Hydration in Vanadia–Titania Catalysts at Low Loading. *J. Phys. Chem. C* **2011**, *115*, 24133–24142.

(46) Popa, C.; Ganduglia-Pirovano, M. V.; Sauer, J. Periodic Density Functional Theory Study of VO_n Species Supported on the CeO_2 (111) Surface. *J. Phys. Chem. C* **2011**, *115*, 7399–7410.

(47) Shapovalov, V.; Metiu, H. VO_x (x = 1−4) Submonolayers Supported on Rutile TiO_2 (110) and CeO_2 (111) Surfaces. *J. Phys. Chem. C* **2007**, *111*, 14179–14188.

(48) Badri, A.; Binet, C.; Lavalley, J.-C. Use of Methanol as an IR Molecular Probe to Study the Surface of Polycrystalline Ceria. *J. Chem. Soc., Faraday Trans.* **1997**, *93*, 1159–1168.

(49) Yang, C.; Bebensee, F.; Nefedov, A.; Wöll, C.; Kropp, T.; Komissarov, L.; Penschke, C.; Moerer, R.; Paier, J.; Sauer, J. Methanol Adsorption on Monocrystalline Ceria Surfaces. *J. Catal.* **2016**, *336*, 116–125.

(50) Song, H.; Bao, X.; Hadad, C. M.; Ozkan, U. S. Adsorption/Desorption Behavior of Ethanol Steam Reforming Reactants and Intermediates over Supported Cobalt Catalysts. *Catal Lett* **2011**, *141*, 43–54.

(51) Mullins, D. R.; Senanayake, S. D.; Chen, T.-L. Adsorption and Reaction of C_1 −C_3 Alcohols over CeO_X (111) Thin Films. *J. Phys. Chem. C* **2010**, *114*, 17112–17119.

(52) Li, M.; Wu, Z.; Overbury, S. H. Surface Structure Dependence of Selective Oxidation of Ethanol on Faceted CeO_2 Nanocrystals. *J. Catal.* **2013**, *306*, 164–176.

(53) Yee, A.; Morrison, S. J.; Idriss, H. A Study of the Reactions of Ethanol on CeO_2 and Pd/CeO_2 by Steady State Reactions, Temperature Programmed Desorption, and In Situ FT-IR. *J. Catal.* **1999**, *186*, 279–295.

(54) Sheng, P.-Y.; Bowmaker, G. A.; Idriss, H. The Reactions of Ethanol over Au/CeO_2. *Appl. Catal. A* **2004**, *261*, 171–181.

(55) Hussein, G. A. M.; Sheppard, N.; Zaki, M. I.; Fahim, R. B. Infrared Spectroscopic Studies of the Reactions of Alcohols over Group IVB Metal Oxide Catalysts. *J. Chem. Soc., Faraday Trans.* **1991**, *87*, 2661–2668.

(56) Finnie, K. S.; Luca, V.; Moran, P. D.; Bartlett, J. R.; Woolfrey, J. L. Vibrational Spectroscopy and EXAFS Study of $Ti(OC_2H_5)_4$ and Alcohol Exchange in $Ti(iso\text{-}OC_3H_7)_4$. *J. Mater. Chem.* **2000**, *10*, 409–418.

(57) Siokou, A.; Nix, R. M. Interaction of Methanol with Well-Defined Ceria Surfaces. *J. Phys. Chem. B* **1999**, *103*, 6984–6997.

(58) Badri, A.; Binet, C.; Lavalley, J.-C. An FTIR Study of Surface Ceria Hydroxy Groups During a Redox Process with H_2. *J. Chem. Soc., Faraday Trans.* **1996**, *92*, 4669-4673.

(59) Moncada, J.; Adams, W. R.; Thakur, R.; Julin, M.; Carrero, C. A. Developing a Raman Spectrokinetic Approach To Gain Insights into the Structure−Reactivity Relationship of Supported Metal Oxide Catalysts. *ACS Catal.* **2018**, *8*, 8976-8986.

TOC graphic

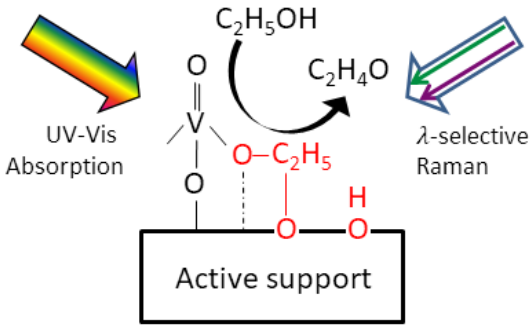
C2H5OH
C2H4O
O
V
O
O–C2H5
H
O
O
UV-Vis
Absorption
λ-selective
Raman
Active support